PERIODICO di MINERALOGIA
established in 1930

DIPARTIMENTO
DI SCIENZE DELLA TERRA

SAPIENZA
UNIVERSITÀ DI ROMA

An International Journal of
Mineralogy, Crystallography, Geochemistry,
Ore Deposits, Petrology, Volcanology
and applied topics on Environment, Archaeometry and Cultural Heritage

The crystal structure of mineral fibres. 3. Actinolite asbestos

Simone Pollastri [a,*], Lara Gigli [b], Paolo Ferretti [c], Giovanni B. Andreozzi [d], Nicola Bursi Gandolfi [a], Kilian Pollok [e], Alessandro F. Gualtieri [a]

[a] Department of Chemical and Geological Sciences, University of Modena and Reggio Emilia, Via Campi 103, I-41125 Modena, Italy
[b] Elettra-Sincrotrone Trieste S.C.p.A., Strada Statale 14 - km 163,5 in AREA Science Park, 34149 Basovizza, Trieste, Italy
[c] MUSE - Trento museum of Sciences, Corso del Lavoro e della Scienza 3, I-38122 Trento, Italy
[d] Department of Earth Sciences, Sapienza University of Rome, Piazzale Aldo Moro 5, I-00185 Roma, Italy
[e] Institut für Geowissenschaften Mineralogie, Friedrich-Schiller-Universität Jena, Carl-Zeiss-Promenade 10, D-07745 Jena, Germany

ARTICLE INFO

Submitted: March 2017
Accepted: April 2017
Available on line: May 2017

* Corresponding author:
simone.pollastri@unimore.it

DOI: 10.2451/2017PM714

How to cite this article:
Pollastri S. et al. (2017)
Period. Mineral. 86, 89-98

ABSTRACT

The present work reports chemical and structural data of actinolite asbestos from Aurina Valley, Bolzano (Italy). The chemical composition was determined using EMPA and TG analysis, and the Fe^{3+}/Fe_{tot} ratio was accurately evaluated with independent ^{57}Fe Mössbauer spectroscopy. Morphology and crystallinity were also investigated through SEM and TEM investigations. Crystal structure was refined using high-resolution synchrotron XRPD data. The iron content of Aurina Valley sample is lower compared to two representative asbestiform actinolite samples (with structure refinement) taken from the literature (FeO_{tot} 7.77 wt% against 12÷13 wt%, respectively), accounting for the reduced cell volume here measured (910.29 Å³ against 912÷918 Å³, respectively). Refined site scattering values of Aurina Valley sample are in agreement with those calculated from chemical compositions, and the optimized structural formula is:
$K_{0.02}Na_{0.05}(Na_{0.08}Ca_{1.92})_{\Sigma=2.00}(Mg_{3.80}Fe^{2+}_{0.79}Fe^{3+}_{0.11}Al_{0.20}Mn_{0.05}Ni_{0.02}Cr_{0.01})_{\Sigma=4.98}(Si_{7.67}Al_{0.25})_{\Sigma=7.92}O_{21.69}(OH)_{2.31}$.
The C sites *M*(1), *M*(2) and *M*(3) are occupied by Mg and Fe in a proportion of ~4:1, whereas the *M*(4) site contains mainly Ca and a very small amount of Na. Iron exclusively occupies the octahedral C sites, with Fe^{2+} ions occurring at the *M*(1,2,3) sites and the small amount of Fe^{3+} (13% of Fe_{tot}) ordered at the *M*(2) site. The refined crystal structure and cation distribution are fully consistent with results previously obtained on asbestiform and non-asbestiform samples belonging to the tremolite-actinolite-ferro–actinolite substitutional series.

Keywords: actinolite; amphibole asbestos; Rietveld; crystal structure; iron.

BACKGROUND

Actinolite [$\square Ca_2(Mg_{4,5-2,5}Fe^{2+}_{0,5-2,5})Si_8O_{22}(OH)_2$] is a *C*2/*m* monoclinic amphibole which belongs to the tremolite-actinolite-ferro-actinolite substitutional series [$\square Ca_2(Mg,Fe^{2+})_5Si_8O_{22}(OH)_2$].

Amphiboles are double-chain silicates with a Si(Al):O ratio of 4:11 with simplified general formula: $A_{0-1}B_2C_5T_8O_{22}W_2$ (Hawthorne et al., 2012). The oxygen atoms of the chains can coordinate Si(Al) and also a variety of other cations sites. In *C*2/*m* monoclinic amphiboles, the anions W (OH, F, Cl, O^{2-}) occur at the O(3) site, T (Si^{4+}, Al^{3+}) are the tetrahedrally coordinated sites within the

silicate chain, the C cations (Mg^{2+}, Fe^{2+}, Mn^{2+}, Al^{3+}, Fe^{3+}, Ti^{3+}, Ti^{4+} Li^{+}, Mn^{3+}) occur at the octahedrally coordinated sites *M*(1), *M*(2) and *M*(3), the B cations (Na^{+}, Li^{+}, Ca^{2+}, Mn^{2+}, Fe^{2+}, Mg^{2+}) occur at the [8]-coordinated *M*(4) site, and the A cations (Na^{+}, K^{+}, Ca^{2+}, Li^{+}) occur in the large [12]-coordinated *A* cavity with a complex nomenclature which reflects its positional disorder (Hawthorne et al., 2012).

In addition to the prismatic variety, the fibrous-asbestiform variety of actinolite belongs to the regulated asbestos minerals, together with amosite, anthophyllite asbestos, crocidolite, chrysotile and tremolite asbestos (IARC, 1973; USGS, 2001). It is now well known that the inhalation of asbestos minerals can cause the onset of malignant lung diseases (mainly lung carcinoma and pleural/peritoneal malignant mesothelioma, MM; see for reviews: Broaddus et al., 2011; Bunderson-Schelvan et al., 2011; Gulati and Redlich, 2015; Huang et al., 2011; Mossman et al., 2011; Roe and Stella, 2015), but the mechanisms by which they induce cyto- and geno-toxic damage remain ambiguous. The great chemical variability, fibre size, surface reactivity, biopersistence, iron oxidation state/coordination number all play a synergetic role and contribute to make the understanding of the biogeochemical reactions extremely difficult (Fubini and Mollo, 1995; Hardy and Aust, 1995; Donaldson et al., 2010).

A full mineralogical and crystallographic characterization of the main mineral fibres (namely those of socio-economic and industrial relevance) is of paramount importance and can be used as a basis to understand the chemical/physical and biological properties relevant to toxicity and pathogenicity. To achieve this goal, a long term research project under the Italian Research Project of National Interest (PRIN) is in progress since 2011. The ultimate aim of the project is the development of a general model capable of describing the fibre toxicity that can be predictive to assess the potential toxicity and pathogenicity of unregulated fibres, preventing new cases of mass exposure as those reported in the past for the F-edenite (Comba et al., 2003) and fibrous erionite (Dumortier et al., 2001).

This work (the last of three focused on the crystal structure of the mineral fibres; Pollastri et al. 2016, 2017) is a part of the aforementioned PRIN project and follows the research line of the crystal chemical characterization of fibrous amphiboles such as fluoro-edenite (Gianfagna et al., 2003; Gianfagna et al., 2007; Andreozzi et al., 2009) fibrous tremolite (Ballirano et al., 2008; Pacella et al., 2008) fibrous richterite (Pacella and Ballirano, 2016) and winchite (Gunter et al., 2003).

The sample that we have selected for the study is from Aurina Valley, Bolzano (Italy) and displays particles with both fibrous and acicular crystal habit. We have adopted the World Health Organization - WHO (1997) definitions based on dimensional characters, and consider a "fibre" as an elongated particle with length ≥5 μm, diameter ≤3 mm, length/diameter (aspect) ratio ≥3:1, uniform parallel sides and geometrical faces. Because most of the particles fulfils the WHO (1997) dimensional criteria, our sample has a "fibrous" crystal habit. The sample also contains minor elongated particles that do not fulfil the WHO (1997) dimensional criteria, showing a needle-like crystal habit. For such particles the correct classification is "acicular crystal habit". The definition of asbestos that we have adopted are not based on physical properties of the specimen like flexibility or presence of fibre bundles, although we have also found many fibrils in the sample that are characteristic of an asbestos aerosol. Thus, for the present study, we have decided to follow the recommendations of the WHO (1997) and International Mineralogical Association (Leake 1978), classifying our sample as actinolite asbestos. Because some of the fibres present an acicular crystal habit, this variety of actinolite may also be termed as 'byssolite' (Dana,1932; Verkouteren and Wylie, 2000) although this term is now dismissed.

The sample was fully characterized with Electron Micro-Probe Analysis (EMPA), ^{57}Fe Mössbauer spectroscopy (MS), field emission gun Scanning Electron Microscopy (FEG-SEM), Transmission Electron Microscopy (TEM) and synchrotron X-Ray powder-diffraction (XRPD). A special attention was paid to the speciation and site occupancy of iron because it is considered to play a major role in the pathogenicity of the fibres. In fact, it is well known that active surface ferrous iron may promote generation of reactive oxygen species (ROS), responsible of cito- and geno-toxicity effects (Hardy and Aust, 1995; Fantauzzi et al., 2010, 2012; Pacella et al., 2012, 2014, 2015).

MATERIAL AND METHODS

The sample selected for the study is an asbestos actinolite with ideal formula $\square Ca_2Fe^{2+}_5[Si_8O_{22}](OH)_2$ and space group *C*2/*m*, from Aurina Valley, Bolzano (Italy). Pure fibres from the natural sample were manually selected under the optical microscope and cross-checked with XRPD (using a conventional source).

EMPA and thermogravimetric (TG) analysis

EMPA for quantitative chemical composition of the sample were performed using two instruments: a JEOL JXA-8230, with accelerating voltage of 15 kV and 5 μm spot size (available at the department of Mineralogy of the Friedrich Schiller University of Jena, Germany) and a JEOL 8200 Super Probe instrument with W hairpin type filament and minimum accelerating voltage of 30 kV (available at the department of Earth Sciences "Ardito Desio" of the University of Milano, Italy). Analysis were performed on accurately selected fibres (see above) so

that estimates should be highly reliable.

For the determination of structural water, thermogravimetry (TG), differential thermogravimetry (DTG) and DTA were performed on the sample using a simultaneous differential thermal analysis (SDTA) SEIKO SSC/5200 SII. Data were collected in air with a flow rate of 2 μL/min, in the range 25-1150 °C, and heating rate of 10 °C/min.

^{57}Fe Mössbauer spectroscopy

The Fe^{3+}/Fe_{tot} ratio was accurately determined using ^{57}Fe Mössbauer spectroscopy. For the measurement, the fibres were ground in an agate mortar and mixed with a powdered acrylic resin to avoid preferred orientations. The FeO total content was 7.8 wt%, and about 50 mg of sample were used, so that the absorber was within the limits for the thin absorber thickness described by Long et al. (1983). Data were collected at room temperature, using a conventional spectrometer operated in constant acceleration mode, with a ^{57}Co source of nominal strength of 50 mCi in a rhodium matrix, and recorded in a multichannel analyzer using 512 channels for the velocity range -4 to 4 mm/s. About 3.5 million counts per channel were collected. After velocity calibration against a spectrum of high-purity α-iron foil (25μm thick), the raw data were folded to 256 channels. The spectrum was fitted using the Recoil 1.04 fitting program (Lagarec and Rancourt, 1988). Pure Lorentian line shape were fitted, and results were satisfactory (reasonable parameters and reduced χ^2=0.62). On this basis, more complex fitting, involving quadrupole splitting distributions was considered unnecessary. A model based on three doublets, with two doublets for Fe^{2+} and one doublet for Fe^{3+} was chosen. Uncertainties were calculated using the covariance matrix and the errors were estimated to be approximately ±3% for both Fe^{2+} and Fe^{3+} quantification (Table 2).

Electron microscopy FEG-SEM and TEM

SEM was performed using a FEI Nova NanoSEM 450 equipped with a X-EDS Bruker QUANTAX-200 system. Images were obtained using backscattered electrons (BSE) mode from fibres mounted on an Al sample stub and gold coated (about 10nm of thickness). Analytical conditions were 15kV accelerating voltage and 3.5 μA beam current.

TEM investigations were performed using a TEM/STEM FEI Tecnai G^2 200 kV instrument, at the Friedrich-Schiller University of Jena. Sample was gently ground in an agate mortar with ethanol and then a droplet of suspension was deposited on a Cu TEM grid with a carbon network as support film.

Synchrotron XRPD

An high-resolution XRPD pattern was collected at the MCX beamline at ELETTRA (Trieste, Italy) using a Debye-Scherrer geometry and a wavelength of 1.0324 Å. Sample has been manually ground in an agate mortar and the powders were inserted in a borosilicate 0.3 mm diameter capillary that was made spun during the data collection.

Preliminary quantitative phase analysis were performed using the Rietveld method (Rietveld, 1969) implemented in the GSAS package (Larson and Von Dreele, 1994) and its graphical interface EXPGUI (Toby, 2001). Rietveld structural refinements were also performed with GSAS/EXPGUI, using one of the structures of Evans and Yang (1998) as a starting structural model.

In GSAS, the structure factors were calculated using the formal scattering factors for neutral atoms. The background profile was fitted with a Chebyshev polynomial function with 32 coefficients due to the complexity of the background curve originated by the glass capillary. The diffraction peak profiles were modelled using a pseudo-Voigt function with a θ-independent Gaussian and two θ-dependent Lorentzian coefficients. The unit-cell parameters and phase fractions were refined together with the atomic coordinates, the atomic site occupancies, and the isotropic atomic displacement parameters. Soft constraints on tetrahedral bond lengths were imposed and used as additional observations in the earlier stages of the refinement procedure. The weight of the constraints was progressively reduced to 40 in the later stages.

RESULTS AND DISCUSSION

Figure 1 a,b are SEM-FEG images showing both the fibrous and acicular crystal habit, length and aspect ratios of the sample whereas Figure 2 reports an high resolution TEM image and indexed electron diffraction spots evidencing the high crystallinity and the absence of extensive linear disorder (e.g. dislocations).

The EMPA chemical composition of the sample in oxides (wt%) is reported in Table 1. Impurities were searched combining the EMPA results, the ^{57}Fe-Mössbauer and the XRPD qualitative/quantitative phase analysis, but the sample can be considered pure within the detection limits of the experimental conditions used for the X-ray diffraction experiment. Indeed, the Mössbauer pattern is typical of a paramagnetic material without impurities and both Fe^{2+} and Fe^{3+} show hyperfine parameters typical of octahedral coordination (Figure 3 and Table 2).

EMPA data, together with the water content from TG analysis and the quantification of Fe^{2+} and Fe^{3+} using independent Mössbauer data, allowed the calculation of the following crystal-chemical formula, normalized on the basis of 24 O:

$K_{0.02}Na_{0.05}(Na_{0.08}Ca_{1.92})_{\Sigma=2.00}(Mg_{3.80}Fe^{2+}_{0.79}Fe^{3+}_{0.11}Al_{0.20}Mn_{0.05}Ni_{0.02}Cr_{0.01})_{\Sigma=4.98}(Si_{7.67}Al_{0.25})_{\Sigma=7.92}O_{21.69}(OH)_{2.31}$

Cations reported in atoms per formula unit (a.p.f.u.)

were assigned following the schemes proposed by Hawthorne and Oberti (2007) and Leake et al. (1997).

Figure 4 reports the graphical output of the Rietveld refinement. The agreement factors of the refinement (as defined in Larson and Von Dreele, 1994) and calculated unit cell parameters are reported in Table 3. Fractional coordinates, isotropic displacement parameters (Å^2) and site scattering values obtained from the structure refinement are reported in Table 4 whereas relative selected bond distances and polyhedral distortion ($\Delta x10^4$) for the *T* and *M* sites are reported in Table 5.

Table 1. Chemical composition of asbestos actinolite from EMPA analysis. Reported chemical compositions are mean values of analyses carried out on 10 different fibres with the JEOL 8200 and on 26 different fibres with the JEOL JXA-8230. Reference data of Evans and Yang (1998) (E&Y98; sample 156831) and of Vignaroli et al. (2014) (Vigna14; sample LIV335) are shown for comparison.

Oxides	This work	E&Y98	Vigna14
SiO_2	54.83 (5)	54.84	55.14
TiO_2	0.037 (9)	0.01	0.03
Al_2O_3	2.70 (6)	1.16	1.83
Cr_2O_3	0.08 (9)	-	0.01
MnO	0.40 (7)	0.45	0.15
MgO	18.21 (3)	15.68	15.77
CaO	12.77 (6)	12.47	11.85
Na_2O	0.48 (6)	0.16	0.53
K_2O	0.13 (3)	0.03	0.04
NiO	0.18 (2)	-	-
F	-	-	0.07
Fe_{tot}	7.77 (5)	12.89	12.28
FeO	6.76 (5)*	11.61	10.98
Fe_2O_3	1.01 (5)*	1.28	1.48
H_2O	2.47**	2.00	2.06
Total	100.06	99.69	99.76

*Partition determined from Mössbauer data;**determined from TG data.

The refined site scattering values obtained from the structure refinement are in agreement with those calculated from the chemical composition (Table 4). The Mg/(Mg+Fe) ratio of 0.84 calculated from the Rietveld refinement is in agreement with that of 0.80 obtained from the chemical data; the difference between the two values should be attributed to the other cations present in the *M* sites (Al, Mn, Ni and Cr), not considered in the refinement. As a first conclusion, the optimised crystal-chemical formula contains minor Fe^{3+}, minor amounts of K and Na and a calculated Mg/(Mg+Fe) ratio of 0.80 which, according to amphibole nomenclature (Hawthorne et al. 2012), allows the Aurina Valley fibrous amphibole to be classified as 'actinolite'.

The first papers reporting the crystal structure of an actinolite sample are those of Zussman (1955) and Zussman (1959) whereas a more complete work focussed on the structure of a prismatic actinolite sample and other *C*/2*m* amphiboles is reported by Mitchell et al. (1970). More recently, Evans and Yang (1998) have conducted an accurate study on the tremolite-actinolite-ferro-actinolite series, but samples were probably not fibrous. Chemistry and structure of fibrous actinolite samples (more similar to our sample) from the Ligurian Alps (Italy) have also been recently reported by Vignaroli et al. (2014).

The result obtained indicates that Mg and Fe^{2+} are disordered over the C sites, whereas all the Fe^{3+} was allocated at the *M*(2) site, considering its shorter bond-length of 2.075 (Table 5) and according to Evans and Yang (1998). A similar picture was found also by Vignaroli et al. (2014), because, even if they observed a site-preference for Fe^{2+} in the octahedrally coordinated sites with *M*(2)>*M*(1)>*M*(3), considering the site multiplicity, similar to that of tremolite, its distribution is almost disordered over all these sites (Ballirano et al., 2008;

Table 2. Room temperature ^{57}Fe Mössbauer hyperfine parameters of the analyzed sample. The value of the reduced χ^2 is 0.62.

Sample	δ (mm/s)	ΔE_Q (mm/s)	Γ (mm/s)	Assignment	Area (%)	Fe^{3+}_{corr} (% Fe_{tot})
Fibrous actinolite, Aurina Valley	1.14	2.87	0.36	Fe^{2+}	49	13
	1.14	2.03	0.50	Fe^{2+}	36	
	0.32	0.82	0.40	Fe^{3+}	12	
	0.32	0.10	0.30	Fe^{3+}	3	

Note: Center shift (δ) measured with respect to α-iron. Lorentzian site analysis: uncertainties were estimated at no less than ±0.02 mm/s for center shift, quadrupole splitting (ΔE_Q) and full width at half maximum (Γ), and ±3% for absorption area. The Fe^{3+}_{corr} is obtained from the raw value by applying the correction factors of Dyar et al. (1993).

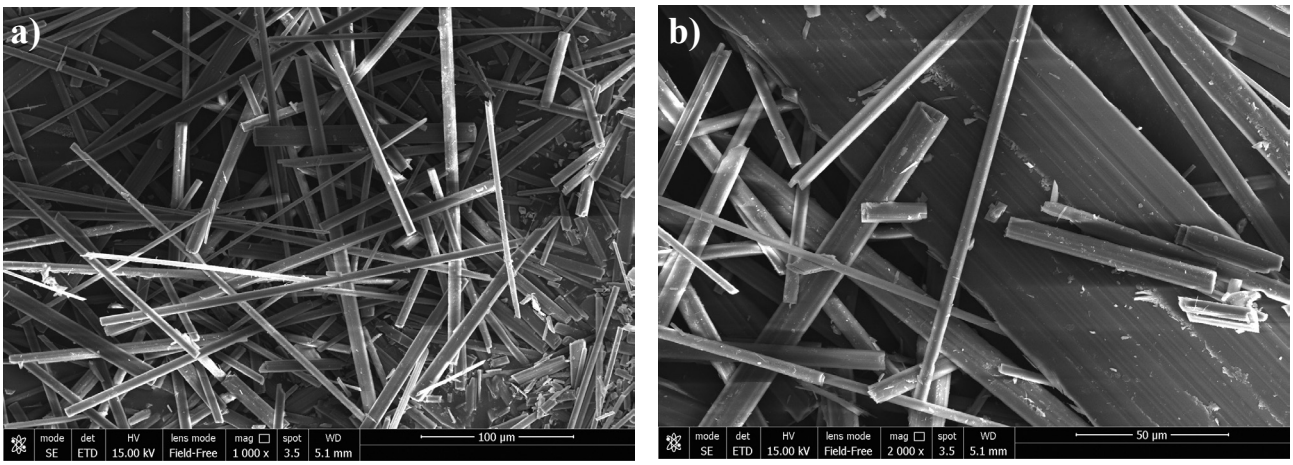

Figure 1. High resolution FEG–SEM images of actinolite asbestos from Aurina Valley: a) Dimension bar 100 µm; b) Dimension bar 50 µm.

Pacella et al., 2008; Pacella et al., 2010). Concerning Fe^{3+}, a systematic site-preferences has not been observed by these authors. All the Na and Ca present in the sample has been allocated in the A and *M*(4) sites, in [8]-fold coordinated environment. For our sample, we have not the problem of allocating Mn, being ≤0.05 apfu.

All the refined cell parameters and volume (Table 3) are smaller than those of Evans and Yang (1998) and Vignaroli et al. (2014) because of the lower iron content of our sample (Fe/Fe+Mg % ratio of 0.44 and 0.45 with respect to our of 0.30). Nevertheless, our parameters are perfectly in line with the trends observed for the tremolite-actinolite-ferro-actinolite series (Figures 4, 5 and 6 in Verkouteren and Wylie, 2000).

Considering cell parameters, volume and bond distances (Tables 3 and 5, respectively) our data are similar to the sample LIV335 studied by Vignaroli et al. (2014), although our *M* sites display smaller polyhedron distorsion. Nevertheless, as can be seen in the plot of Figure 5, that is a modified version after Evans and Yang (1998), our cell parameters (red star) are in line with the other literature data along the tremolite-actinolite serie, in relation to macroscopic (Fe+Mn)/(Fe+Mn+Mg) % ratio.

Refined distances of 1.634 Å for <*T*(1)-O> and 1.636 Å for <*T*(2)-O> are consistent with the occurrence of ca. 0.2-0.3 a.p.f.u. tetrahedrally coordinated Al (Figure 17 in Hawthorne and Oberti, 2007) and in perfect agreement with chemical data. Polyhedral distortion Δ shows very small value for *T*(1) whereas it is larger for *T*(2) (Table 5)

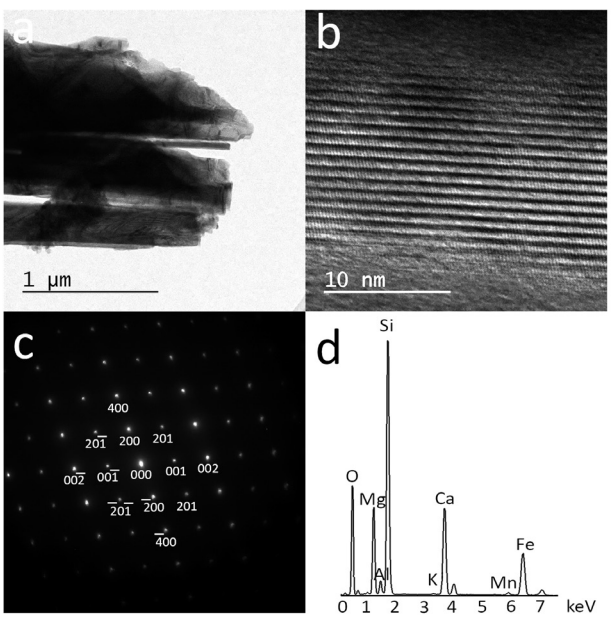

Figure 2. Results of the TEM analysis on the actinolite asbestos sample: a) TEM image of a fibre at low magnification; b) High resolution TEM image of the same fibre; c) Indexed electron diffraction pattern; d) EDS spectra collected on the same fibre.

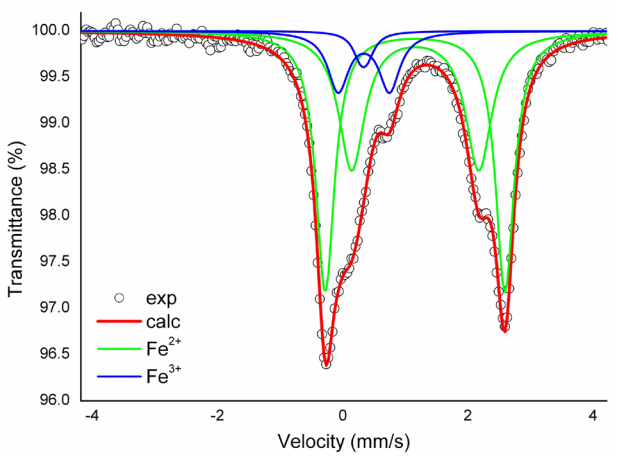

Figure 3. Room temperature ^{57}Fe Mössbauer spectrum of actinolite asbestos.

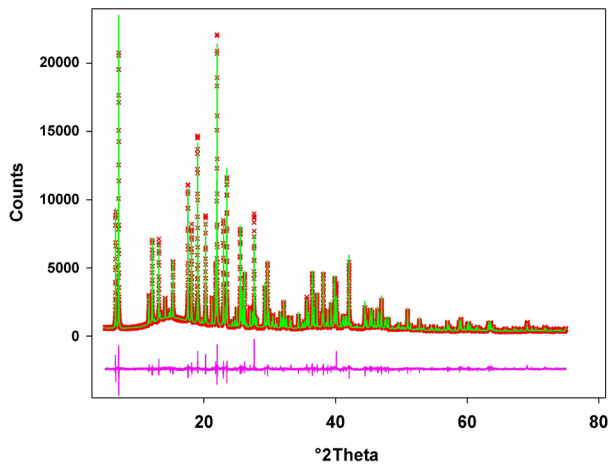

Figure 4. Rietveld refinement of actinolite asbestos. Observed (red crosses), calculated (continuous greed line), and difference (violet bottom line) curves are reported.

Table 3. Unit cell parameters and agreement factors of the refinement for our actinolite sample. Reference data of Evans and Yang (1998) (E&Y98; sample 156831) from single-crystal and of Vignaroli et al. (2014) (Vigna14; sample LIV335) from XRPD Rieveld refinement are shown for comparison.

	This work	Vigna14	E&Y98
a (Å)	9.84896(4)	9.8527(2)	9.881(1)
b (Å)	18.07748(8)	18.0920(4)	18.139(2)
c (Å)	5.28860(2)	5.29042(11)	5.298(1)
β (°)	104.817(2)	104.729(2)	104.78(1)
V (Å3)	910.294(7)	912.06(4)	918.1
R_{wp}	6.19 %	6.12 %	0.041*
R_p	4.69 %	4.83 %	0.036*
X^2	3.33	1.17	**

*R_w and R parameters for single-crystal X-ray diffraction refinements.**Not reported in the reference paper.

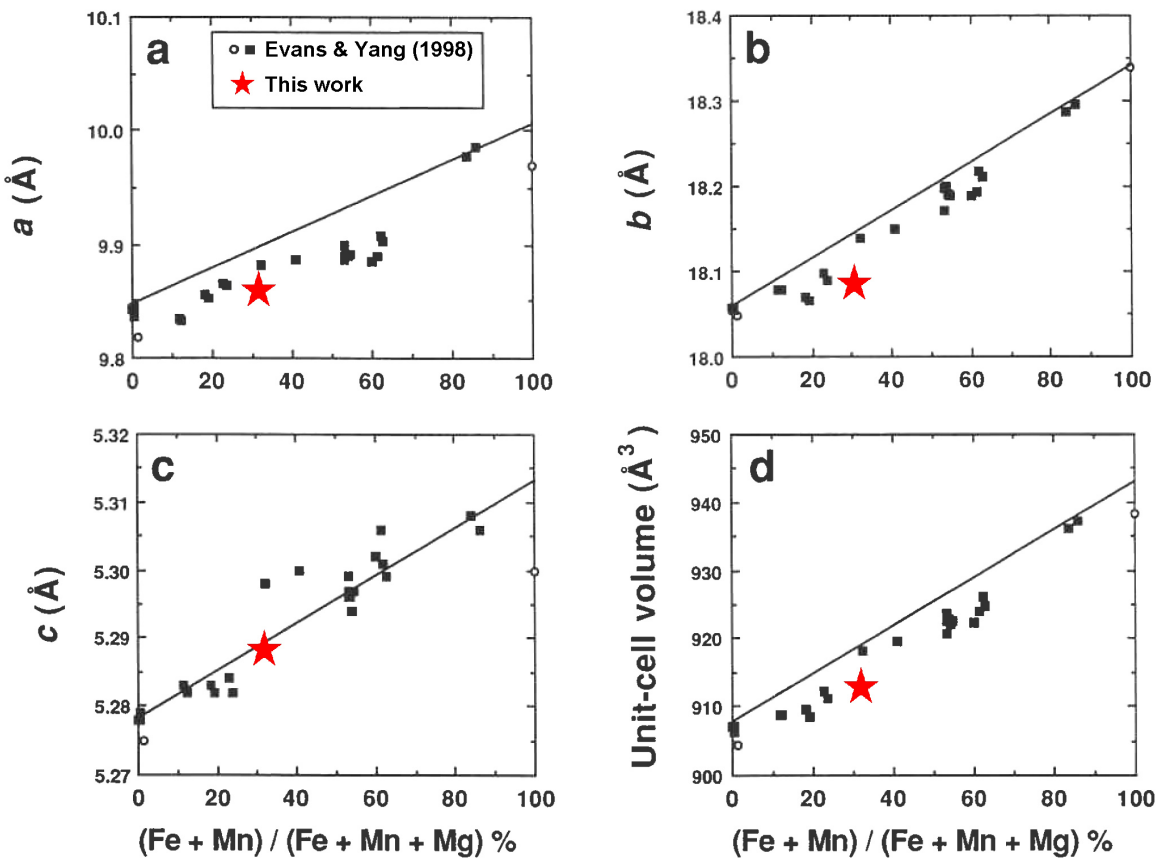

Figure 5. Figure modified after Evans and Yang (1998), showing the dependence of the unit cell parameters along the tremolite-actinolite series vs. macroscopic (Fe+Mn)/(Fe+Mn+Mg)% ratio.
Black squares and circles= Data reported by Evans and Yang (1998); red star= Our actinolite sample.

Table 4. Final atomic coordinates, occupancies and atomic displacement parameters (Å^2) for asbestos actinolite.

site	*x/a*	*y/b*	*z/c*	U_{iso}
Am	0.0053(118)	½	-0.0596(118)	0.0500*
M(1)	0	0.08779(11)	½	0.01816(82)
M(2)	0	0.17660(11)	0	0.01339(76)
M(3)	0	0	0	0.0138(10)
M(4)	0	0.277833(89)	½	0.02110(57)
T(1)	0.27996(19)	0.084232(84)	0.29621(36)	0.02516(60)
T(2)	0.28909(22)	0.171485(88)	0.80671(36)	0.02275(59)
O(1)	0.11107(30)	0.08736(12)	0.21618(50)	0.0135(13)
O(2)	0.12013(33)	0.17117(17)	0.72598(55)	0.0173(12)
O(3)	0.11212(40)	0	0.71660(85)	0.0063(16)
O(4)	0.36519(29)	0.24893(13)	0.78852(63)	0.0137(12)
O(5)	0.34832(38)	0.13497(15)	0.10235(61)	0.02112(98)
O(6)	0.34257(38)	0.11793(14)	0.59227(62)	0.0242(11)
O(7)	0.34149(43)	0	0.29759(86)	0.0137(15)
H*	0.21531(181)	0	0.7353(120)	0.0300*

	Refinement	Site partition	Chemical data
M(1)	8.84	$Fe^{2+}_{0.34(1)}$	
	19.92	$Mg_{1.66(1)}$	
M(2)	5.46	$Fe^{2+}_{0.21(1)}$	
	2.25	$Fe^{3+}_{0.09(1)}$	
	20.40	$Mg_{1.70(1)}$	
M(3)	4.16	$Fe^{2+}_{0.16(1)}$	
	10.08	$Mg_{0.84(1)}$	
C site sum	71.11		73.31
M(4)	0.88	$Na_{0.08(1)}$	
	38.4	$Ca_{1.92(1)}$	
B site sum	39.28		39.28
A site	0.38	$K_{0.02(1)}$	
	0.55	$Na_{0.05(1)}$	
A site sum	0.93		0.93

*Fixed values

in agreement with Vignaroli et al. (2014).

The mean <*M*(1,2,3)-O> is 2.082 Å and considering an empirical ionic radius of 0.78 Å for Fe^{2+}, 0.645 Å for Fe^{3+} and 0.72 Å for Mg, all in octahedrally coordinated environment (Shannon, 1976), our data are in agreement with the estimated dependence of the <*M*(1,2,3)-O> distance as a function of the mean aggregate radius of the *M*(1,2,3) cations in C2/m amphiboles (Figure 21a in Hawthorne and Oberti, 2007). Again, because of the lower iron content of our sample, <*M*(1,2,3)-O> is shorter than the value of 2.086 and 2.089 Å reported by Vignaroli et al. (2014) and Evans and Yang (1998), respectively.

The situation is clearly different for the *M*(4) site which occurs at the junction of the strip of octahedra and the double-chain of tetrahedra in all amphibole structure types, and is occupied almost exclusively by Ca^{2+} (with

Table 5. Selected bond distances (in Å) and polyhedral distortion (Δ x 10^4) for fibrous actinolite. Reference data of Evans and Yang (1998) (E&Y98; sample 156831) from single-crystal and of Vignaroli et al. (2014) (Vigna14; sample LIV335) from XRPD Rieveld refinement are shown for comparison.

		This work	E&Y98	Vigna14			This work	E&Y98	Vigna14
T(1)	- O1	1.60911(1)	1.610(2)	1.594(9)	*T*(2)	- O2	1.60877(1)	1.619(2)	1.642(10)
	- O5	1.64278(0)	1.637(2)	1.629(11)		- O4	1.60247(1)	1.585(2)	1.593(9)
	- O6	1.64595(1)	1.638(2)	1.632(9)		- O5	1.65954(1)	1.659(2)	1.665(9)
	- O7	1.63819(1)	1.623(1)	1.636(6)		- O6	1.67519(0)	1.673(2)	1.651(10)
	average	1.63401	1.627	1.623		average	1.63649	1.634	1.634
	Δ	0.802	0.497*	1.07		Δ	3.692	4.468*	3.31
M(1)	- O1 x2	2.07112(1)	2.083(2)	2.088(10)	*M*(2)	- O1 x2	2.11342(1)	2.143(2)	2.147(9)
	- O2 x2	2.09207(1)	2.099(2)	2.092(9)		- O2 x2	2.09441(1)	2.103(2)	2.074(10)
	- O3 x2	2.09841(1)	2.104(2)	2.087(7)		- O4 x2	2.01661(1)	2.019(2)	2.013(8)
	average	2.08720	2.095	2.089		average	2.07481	2.088	2.078
	Δ	0.312	0.183*	0.01		Δ	4.075	6.123*	6.95
M(3)	- O1 x4	2.08753(1)	2.086(2)	2.111(8)	*M*(4)	-O2 x2	2.41310(1)	2.399(2)	2.366(9)
	- O3 x2	2.07660(1)	2.079(3)	2.052(12)		-O4 x2	2.31548(1)	2.323(2)	2.332(10)
						-O5 x2	2.74452(1)	2.783(2)	2.774(8)
	average	2.08389	2.084	2.091		-O6 x2	2.56505(1)	2.547(2)	2.583(9)
	Δ	0.061	0.025*	1.77		average	2.50954	2.513	2.514
						Δ	41.783	48.752*	50.40
Am	-O5 x2	3.12330(1)							
	-O5 x2	2.87220(1)							
	-O6 x2	2.99911(1)							
	-O7	2.78037(1)							
	-O7	2.19823(1)							
	average	2.87098							
	Δ	94.172							

Note: Polyhedron distortion Δ as defined by Brown and Shannon (1973): $\Delta = (1/n)\Sigma[(R_i-R)/R]^2$ where n is the number of ligands. R is the average bond length and Ri an individual bond length. *Calculated for this work.

a small amount of Na^{2+}) in our sample. The B cation at the *M*(4) site bonds to oxygen atoms of both the strip of octahedra and the double chain of tetrahedra, and is the basic link between these two parts of the structure. As a result, this site and its constituent cations have a major influence on the symmetry, crystal chemistry and chemical composition of the amphiboles (Hawthorne and Oberti, 2007). The distance <*M*(4)-O> of 2.509 Å in our actinolite sample is similar to both that of Vignaroli et al. (2014) and Evans and Yang (1998) (Table 5); similarly to the <*M*(1,2,3)-O> distances, our slightly shorter value is probably due to the lower iron content of our sample. The [8]fold-coordinated environment of Ca^{2+} at the *M*(4) site results distorted (Δ=41.78) but still smaller with respect to that of 48.75 and 50.40 (Table 5) of Evans and Yang (1998) and of Vignaroli et al. (2014), respectively.

CONCLUSIONS

The crystal structure of asbestos actinolite from Aurina Valley (Italy) was determined through Rietveld structural refinement, with the chemical composition determined through EMPA and TG data, and Fe^{3+}/Fe_{tot} ratio measured using ^{57}Fe Mössbauer spectroscopy. Refined site scattering values of Aurina Valley sample are in agreement with

those calculated from chemical compositions.

On this basis, the Mg/(Mg+Fe) ratio is 0.80 which allows, according to amphibole nomenclature, the Aurina fibrous amphibole to be classified as 'actinolite'.

The *M*(1), *M*(2) and *M*(3) sites are occupied by Mg and Fe in a proportion close to 4:1, with Fe^{2+} ions occurring at the *M*(1,2,3) sites and Fe^{3+} ions (13% of Fe_{tot}) only occurring at the *M*(2) site. The *M*(4) site basically contains Ca and minor Na (being the only one capable of hosting these larger cations). The refined crystal structure model is consistent with the structure models of other samples belonging to the tremolite-actinolite-ferro–actinolite substitutional series reported in the literature, and the low cell volume measured for Aurina Valley sample is likely due to its low iron content.

ACKNOWLEDGMENTS

This research was conducted within the research project "*Sviluppo di un modello generale di interazioni tra fibre minerali e cellule biologiche*", a part of the comprehensive granted long term Italian Research Project of National Interest (PRIN 2011) entitled "*Interazione fra minerali e biosfera: conseguenze per l'ambiente e la salute umana*". The synchrotron XRPD pattern was collected at the MCX beamline (ELETTRA, Trieste, Italy) during in-house experiments (May 2016). We want to thank Prof. Stefano Poli and Dott. Andrea Risplendente for the EMPA, and Prof. Falko Langenhorst for the TEM and further EMPA. F.L. thanks the Deutsche Forschungsgemeinschaft for funding the TEM via the Gottfried Wilhelm Leibniz programme (LA 830/14-1).

REFERENCES

Andreozzi G.B., Ballirano P., Gianfagna A., Mazziotti Tagliani S., Pacella A., 2009. Structural and spectroscopic characterization of a suite of fibrous amphiboles with high environmental and health relevance from Biancavilla (Sicily, Italy). American Mineralogist 94, 1333-1340.

Ballirano P., Andreozzi G.B., Belardi G., 2008. Crystal chemical and structural characterization of fibrous tremolite from Susa Valley, Italy, with comments on potential harmful effects on human health. American Mineralogist 93, 1349-1355.

Broaddus V.C., Everitt J.I., Black B., Kane A.B., 2011. Non-neoplastic and neoplastic pleural endpoints following fiber exposure. Journal of toxicology and environmental health Part B, Critical reviews 14, 153-178.

Bunderson-Schelvan M., Pfau J.C., Crouch R., Holian A., 2011. Nonpulmonary outcomes of asbestos exposure. Journal of Toxicology and Environmental Health Part B, Critical Reviews 14, 122-152.

Comba P., Gianfagna A., Paoletti L., 2003. Pleural mesothelioma cases in Biancavilla are related to a new fluoro-edenite fibrous amphibole. Archives of Environmental Health: An International Journal 58, 229-232.

Dana E.S., 1932. A textbook of mineralogy, 4th Ed. revised by W.E. Ford, 574 p. Wiley, Inc, New York.

Donaldson K., Murphy F.A., Duffin R., Poland C.A., 2010. Asbestos, carbon nanotubes and the pleural mesothelium: a review of the hypothesis regarding the role of long fibre retention in the parietal pleura, inflammation and mesothelioma. Particle and Fibre Toxicology 7, 1-17.

Dumortier P., Coplü L., Broucke I., Emri S., Selcuk T., De Maertelaer V., De Vuist P., Baris I., 2001. Erionite bodies and fibres in bronchoalveolar lavage fluid (BALF) of residents from Tuzköy, Cappadocia, Turkey. Occupational and Environmental Medicine 58, 261-266.

Evans B.W. and Yang H., 1998. Fe-Mg order-disorder in tremolite–actinolite–ferro-actinolite at ambient and high temperature. American Mineralogist 83, 458-475.

Fantauzzi M., Pacella A., Atzei D., Gianfagna A., Andreozzi G.B., Rossi A., 2010. Combined use of X-Ray Photoelectron and Mössbauer spectroscopic techniques in the analytical characterization of iron oxidation state in amphibole asbestos. Analytical and Bioanalytical Chemistry 396, 2889-2898.

Fantauzzi M., Pacella A., Fournier J., Gianfagna A., Andreozzi G.B., Rossi A., 2012. Surface chemistry and surface reactivity of fibrous amphiboles that are not regulated as asbestos. Analytical and Bioanalytical Chemistry 404, 821-833.

Fubini B. and Mollo L., 1995. Role of iron in the reactivity of mineral fibers. Toxicology Letters 82, 951-960.

Gianfagna A., Andreozzi G.B., Ballirano P., Mazziotti-Tagliani S., Bruni B.M., 2007. Crystal chemistry of the new fibrous fluoro-edenite amphibole of volcanic origin from Biancavilla (Sicily, Italy). Canadian Mineralogist 45, 249-262.

Gianfagna A., Ballirano P., Bellatreccia F., Bruni B., Paoletti L., Oberti R., 2003. Characterization of amphibole fibres linked to mesothelioma in the area of Biancavilla, Eastern Sicily, Italy. Mineralogical Magazine 67, 1221-1229.

Gulati M. and Redlich C.A., 2015. Asbestosis and environmental causes of usual interstitial pneumonia. Current opinion in pulmonary medicine 21, 193-200.

Gunter M.E., Dyar M.D., Twamley B., Foit F.F. Jr., Cornelius C., 2003. Composition, Fe^{3+}/SFe, and crystal structure of nonasbestiform and asbestiform amphiboles from Libby, Montana, U.S.A. American Mineralogist 88, 1970-1978.

Hardy J.A. and Aust A.E., 1995. Iron in asbestos chemistry and carcinogenicity. Chemical Reviews 95, 97-118.

Hawthorne F.C. and Oberti R., 2007. Amphiboles: crystal chemistry. In: Reviews in Mineralogy and Geochemistry, The Mineralogical Society of America and The Geochemical Society 67, 1-54.

Hawthorne F.C., Oberti R., Harlow G.E., Maresch W.V., Martin R.F., Schumacher J.C., Welch M.D., 2012. Nomenclature of the amphibole supergroup. American Mineralogist 97, 2031-2048.

Huang S.X., Jaurand M.C., Kamp D.W., Whysner J., Hei T.K., 2011. Role of mutagenicity in asbestos fiber-induced carcinogenicity and other diseases. Journal of toxicology and environmental health Part B, Critical reviews 14, 179-245.

IARC, 1973. Some inorganic and organometallic compounds. IARC Monographs on the Evaluation of Carcinogenic Risk of Chemicals to Man 2, 1-181.

Larson A.C. and Von Dreele R.B., 1994. Generalized Structure Analysis System. Los Alamos National Lab, New Mexico, LAUR 86-748.

Leake B.E., Woolley A.R., Arps C.E.S., Birch W.D., Gilbert M.C., Grice J.D., Hawthorne F.C., Kato A., Kisch H.J., Krivovichev V.G., Linthout K., Laird J., Mandarino J.A., Maresch V.W., Nickel E.H., Rock N.M.S., Schumacher J.C., Smith D.C., Stephenson N.N., Ungaretti L., Withtaker E.J.W., Youzhi G., 1997. Nomenclature of amphiboles: report of the subcommittee on amphiboles of the International Mineralogical Association, Commission on New Minerals and Mineral Names. American Mineralogist 82, 1019-1037.

Lagarec K. and Rancourt D.G., 1998. RECOIL, Mössbauer spectral analysis software for windows (version 1.0). Department of Physics, University of Ottawa, Canada.

Long G.J., Cranshaw T.E., Longworth G., 1983. The ideal Mössbauer effect absorber thickness. Mössbauer Effect Reference and Data Journal 6, 42-49.

Mitchell J.T., Bloss F.D., Gibbs G.V., 1971. Examination of the actinolite structure and four other *C*2/*m* amphiboles in terms of double bonding. Zeitschrift für Kristallographie-Crystalline Materials 133, 273-300.

Mossman B.T., Lippmann M., Hesterberg T.W., Kelsey K.T., Barchowsky A., Bonner J.C., 2011. Pulmonary endpoints (lung carcinomas and asbestosis) following inhalation exposure to asbestos. Journal of toxicology and environmental health Part B, Critical reviews 14, 76-121.

Pacella A., Andreozzi G.B., Ballirano P., Gianfagna A., 2008. Crystal chemical and structural characterization of fibrous tremolite from Ala di Stura (Lanzo Valley, Italy). Periodico di Mineralogia 77, 51-62.

Pacella A., Andreozzi G.B., Fournier J., 2010. Detailed crystal chemistry and iron topochemistry of asbestos occurring in its natural setting: a first step to understanding its chemical reactivity. Chemical Geology 277, 197-206.

Pacella A., Andreozzi G.B., Fournier J., Stievano L., Giantomassi F., Lucarini G., Rippo M.R., Pugnaloni A., 2012. Iron topochemistry and surface reactivity of amphibole asbestos: relations with in vitro toxicity. Analytical and Bioanalytical Chemistry 402, 871-881.

Pacella A., Fantauzzi M., Turci F., Cremisini C., Montereali M.R., Nardi E., Atzei D., Rossi A., Andreozzi G.B., 2014. Surface modifications and dissolution reactions of UICC crocidolite in buffered solutions at physiological pH: a combined ICP-OES, XPS and TEM investigation. Geochimica et Cosmochimica Acta 127, 221-232.

Pacella A., Fantauzzi M., Turci F., Cremisini C., Montereali M.R., Nardi E., Atzei D., Rossi A., Andreozzi G.B., 2015. Surface alteration mechanism and topochemistry of iron in tremolite asbestos: a step toward understanding the potential hazard of amphibole asbestos. Chemical Geology 405, 28-38.

Pacella A. and Ballirano P., 2016. Chemical and structural characterization of fibrous richterite with high environmental and health relevance from Libby, Montana (USA). Periodico di Mineralogia 85, 169-177

Pollastri S., Perchiazzi N., Lezzerini M., Plaisier J.R., Cavallo A., Dalconi M.C., Bursi Gandolfi N., Gualtieri A.F., 2016. The crystal structure of mineral fibres. 1. Chrysotile. Periodico di Mineralogia 85, 249-259 .

Pollastri S., Perchiazzi N., Gigli L., Ferretti P., Cavallo A., Bursi Gandolfi N., Pollok K., Gualtieri A.F., 2017. The crystal structure of mineral fibres: 2. Amosite and fibrous anthophyllite. Periodico di Mineralogia 86, 55-65 .

Rietveld H.M., 1969. A profile refinement method for nuclear and magnetic structures. Journal of Applied Crystallography 2, 65-71.

Roe O.D. and Stella G.M., 2015. Malignant pleural mesothelioma: history, controversy and future of a manmade epidemic. European respiratory review: an official journal of the European Respiratory Society 24, 115-131.

Shannon R.T., 1976. Revised effective ionic radii and systematic studies of interatomic distances in halides and chalcogenides. Acta crystallographica section A: crystal physics, diffraction, theoretical and general crystallography 32, 751-767.

Toby B.H., 2001. EXPGUI, a graphical user interface for GSAS. Journal of Applied Crystallography 34, 210-213.

USGS, 2001. Some Facts about Asbestos (USGS Fact Sheet FS-012-01), 4 pp.

Verkouteren J.R. and Wylie A.G., 2000. The tremolite-actinolite-ferro-actinolite series: Systematic relationships among cell parameters, composition, optical properties, and habit, and evidence of discontinuities. American Mineralogist 85, 1239-1254.

Vignaroli G., Ballirano P., Belardi G., Rossetti F., 2014. Asbestos fibre identification vs. evaluation of asbestos hazard in ophiolitic rock mélanges, a case study from the Ligurian Alps (Italy). Environmental Earth Sciences 72, 3679-3698.

WHO, 1997. Determination of airborne fibre number concentrations; a recommended method, by phase contrast optical microscopy (membrane filter method). World Health Organization, Geneva, Switzerland.

Zussman J., 1955. The crystal structure of an actinolite. Acta Crystallographica 8, 301-308.

Zussman J., 1959. A re-examination of the structure of tremolite. Acta Crystallographica 12, 309-312.